SPANDIDOS PUBLICATIONS

INTERNATIONAL JOURNAL OF ONCOLOGY 62: 44, 2023

Dual targets of lethal apoptosis and protective autophagy in liver cancer with periplocymarin elicit a limited therapeutic effect

YUANYUAN HAO[1-3*], TAO SONG[1-3*], MINGYE WANG[1], TONGTONG LI[1], CHI ZHAO[4], TING LI[5], YUNLONG HOU[1-3] and HONGJIANG HE[5]

[1]College of Integrated Traditional Chinese and Western Medicine, Hebei University of Chinese Medicine, Shijiazhuang, Hebei 050200; [2]Hebei Yiling Chinese Medicine Research Institute; [3]New Drug Evaluation Center, Shijiazhuang Yiling Pharmaceutical Co., Ltd, Shijiazhuang, Hebei 050035; [4]Hebei Medical University, Shijiazhuang, Hebei 050017; [5]Department of Head and Neck Surgery, Harbin Medical University Cancer Hospital, Harbin, Heilongjiang 150081, P.R. China

Received September 28, 2022; Accepted January 27, 2023

DOI: 10.3892/ijo.2023.5492

Abstract. Cardiac glycosides (CGs) are candidate anticancer agents that function by increasing $[Ca^{2+}]i$ to induce apoptotic cell death in several types of cancer cells. However, new findings have shown that the anti-cancer effects of CGs involve complex cell-signal transduction mechanisms. Hence, exploring the potential mechanisms of action of CGs may provide insight into their anti-cancer effects and thus aid in the selection of the appropriate CG. Periplocymarin (PPM), which is a cardiac glycoside, is an active ingredient extracted from Cortex periplocae. The role of PPM was evaluated in HepG2 cells and xenografted nude mice. Cell proliferation, real-time ATP rate assays, western blotting, cell apoptosis assays, short interfering RNA transfection, the patch clamp technique, electron microscopy, JC-1 staining, immunofluorescence staining and autophagic flux assays were performed to evaluate the function and regulatory mechanisms of PPM *in vitro*. The *in vivo* activity of the PPM was assessed using a mouse xenograft model. The present study demonstrated that PPM synchronously activated lethal apoptosis and protective autophagy in liver cancer, and the initiation of autophagy counteracted the inherent pro-apoptotic capacity and impaired the anti-cancer effects. Specifically, PPM exerted a pro-apoptotic effect in HepG2 cells and activated macroautophagy by initiation of the AMPK/ULK1 and mTOR signaling pathways. Activation of macroautophagy counteracted the pro-apoptotic effects of PPM, but when it was combined with an autophagy inhibitor, the anti-cancer effects of PPM in mice bearing HepG2 xenografts were observed. Collectively, these results indicated that a self-limiting effect impaired the pro-apoptotic effects of PPM in liver cancer, but when combined with an autophagy inhibitor, it may serve as a novel therapeutic option for the management of liver cancer.

Correspondence to: Professor Yunlong Hou, College of Integrated Traditional Chinese and Western Medicine, Hebei University of Chinese Medicine, 3 Xingyuan Road, Shijiazhuang, Hebei 050200, P.R. China
E-mail: houyunlonghrb@hotmail.com

Professor Hongjiang He, Department of Head and Neck Surgery, Harbin Medical University Cancer Hospital, 150 Haping Road, Harbin, Heilongjiang 150081, P.R. China
E-mail: hehongjiang@ems.hrbmu.edu.cn

[*]Contributed equally

Key words: periplocymarin, autophagy, liver cancer, apoptosis, cardiac glycosides

Introduction

According to the 2018 global cancer statistics, liver cancer was the sixth most common cancer and the fourth most deadly type of cancer worldwide, with ~841,000 new cases each year and ~782,000 deaths (1). Major risk factors for liver cancer include hepatitis B virus infection, hepatitis C virus infection, alcohol abuse, non-alcoholic steatohepatitis, aflatoxin exposure and hemochromatosis (2). Liver cancer is characterized by its high degree of invasiveness, poor clinical prognosis, frequent recurrence and low survival rates (3). Surgical resection and transplantation are the mainstay curative treatments for liver cancer; however, most patients are diagnosed with advanced liver carcinoma, which decreases the chances of survival (4). Moreover, liver cancer is resistant to chemotherapeutic drugs, which results in cancer recurrence after conventional treatment (5). Therefore, developing safer and more effective drugs for liver cancer treatment is of marked importance.

Cortex periplocae, an herbal medicine, is the dried root bark of *Periploca sepium* of the *Asclepiadaceae* family, and contains numerous active ingredients, including cardiac glycosides (CGs), sterols, glycosides, esters and aldehydes that are used clinically to treat heart failure and relieve associated symptoms (6,7). Periplocin is one of the main and active constituents isolated from cortex periplocae. Periplocin undergoes hydrolysis and deglycosylation to yield periplocymarin (PPM), which has a potent cardiotonic effect *in vivo* (8,9). An increasing number of studies have reported that CGs

exert more beneficial therapeutic effects than cardiac cardiotonics (10,11). Mounting evidence has shown that CGs have significant anti-inflammatory, anti-tumor, and anti-senescent effects (12-14). In terms of anti-tumor activity, CGs inhibit the proliferation of numerous malignant cell lines and prevent the growth of tumors *in vivo* (15). Moreover, PPM is considered a natural potential anticancer agent with high permeability and independence from P-glycoprotein influence (16). Studies on the mechanism of action of anti-tumor agents indicate that periplocin induces DNA double-strand breaks in liposarcoma cells and activates the ERK1/2-Egr1 signaling pathway in gastric cancer cells, which induces cell apoptosis (17,18).

In addition to the induction of apoptosis, several other programmed cell death patterns can be targeted to eliminate cancer cells. Given the pivotal roles of autophagy in tumorigenesis and progression (19), cell death stimulated by excessive autophagy, a concept of 'autophagic cell death', has been the subject of intense investigation (20-22). A recent study reported that ouabain, a representative CG, induced autophagic cell death in non-small cell lung carcinoma via the JNK signaling pathway (23). Newman *et al* (24) reported that oleander induced tumor cell autophagy via suppression of the AKT/mTOR signaling pathway in a concentration and time-dependent manner. However, recent advances in the understanding of the molecular processes which contribute to autophagy have elucidated the crosstalk between autophagy and apoptosis. In contrast to autophagic cell death, autophagy exerts cytoprotective effects that negatively modulate apoptosis in several physiological and pathological circumstances (25). Therefore, understanding the mechanisms which underlie the relationship between autophagy and apoptosis is crucial for the development of effective cancer treatments.

In the present study, HepG2 cell lines and a xenograft mouse model were used to evaluate the antitumor effects of PPM, by which a novel mechanism of action (MOA) was demonstrated for PPM.

Materials and methods

Compounds. PPM (molecular formula: $C_{30}H_{46}O_8$; molecular weight: 534.3193; cat. no. 127-32-2; purity: ≥98%; Fig. 1A) was purchased from Chengdu Chroma Biotechnology Co., Ltd.

Cell lines and culture. HepG2 human hepatoblastoma cells were purchased from iCell Bioscience Inc. Huh7 human hepatoma cells were purchased from Shanghai Fuheng Biotechnology Co., Ltd. HepG2 and Huh7 cell lines were authenticated by STR profiling. Cells were cultured in DMEM (Gibco; Thermo Fisher Scientific, Inc.) supplemented with 15% fetal bovine serum (Gibco; Thermo Fisher Scientific, Inc.) and 1% (v/v) penicillin/streptomycin at 37˚C in 5% CO_2. For all experiments, $1x10^5$ cells/well were seeded into a 96-well tissue culture plate. After the cells reached 80% confluence, PPM was added to the culture medium for 48 h at concentrations of $1x10^{-5}$, $1x10^{-6}$, $1x10^{-7}$, $1x10^{-8}$ and $1x10^{-9}$ mol/l, and 0 mol/l as the control. Cell viability was evaluated using CellTiter 96® AQueous One Solution Cell Proliferation Assay (cat. no. G3581, Promega Corporation) according to the manufacturer's protocol.

Wound healing assay. HepG2 cells (~$1x10^5$) were seeded in 6-well plates with 2 ml of DMEM (Gibco; Thermo Fisher Scientific, Inc.) with 15% fetal bovine serum (FBS; Gibco; Thermo Fisher Scientific, Inc.) and cultured at 37˚C overnight. Once the cells reached 90% confluence, a linear scratch wound was created using a 100 μl pipette tip. At different time points (0 and 48 h), images were captured using Cytation 5 Cell Imaging Multimode Reader (BioTek Instruments, Inc.) and analyzed using Gen5.0 (BioTek Instruments, Inc.). The scratch area was measured using ImageJ (version 1.8.0; National Institutes of Health) and this was used to calculate the wound healing percentage.

Colony formation assay. A total of $1x10^3$ HepG2 cells/well from both the control and test groups were plated in a six-well plate and allowed to grow for 12 days at 37˚C. The clones were then fixed with 4% paraformaldehyde at room temperature for 20 min. Subsequently, cells were stained with 0.5% crystal violet at room temperature for 10 min. The number of colonies (>50 cells) was manually counted, using light microscopy and images were captured using a digital camera.

Cell migration assay. Migration assays were performed in 24-well, 8 μm pore, Transwell plates (cat. no. 3422, Corning, Inc.). HepG2 cells in the logarithmic growth phase were diluted to $2.5x10^5$ cells/ml and resuspended in 200 μl serum-free DMEM medium (Gibco; Thermo Fisher Scientific, Inc.) treated with PPMin the upper compartment and 660 μl DMEM medium supplemented with 15% FBS (Gibco; Thermo Fisher Scientific, Inc.) was added to the lower compartment. The plate was incubated at 37˚C for 48 h. Each well was then washed twice with PBS and the inner surface of the upper chamber was carefully wiped with a cotton swab. The migrated cells on the lower surface were imaged using an Olympus IX70 inverted microscope (Olympus Corporation) in three randomly selected visual fields and the migrated cells were quantified using ImageJ (version 1.8.0; National Institutes of Health).

3D cell culture and cytotoxic assay. Cells were seeded ($1x10^5$ cells/well) into ultra-low attachment 96 well microplates, centrifuged at 200 x g for 5 min at room temperature and incubated at 37˚C for 4 days to allow the formation of cell spheroids. Half of each culture supernatant was replaced every 2 days. Cells were continuously cultured for 4 days in a 37˚C cell incubator to observe the cell morphology. Spheres were treated with PPM at the aforementioned concentrations for 72 h and at 37˚C. Cell viability was measured using the CellTiter-Glo® 3D Cell Viability Assay (cat. no. G9681, Promega Corporation) according to the manufacturer's protocol. Cell morphology was assessed on days 2 and 3 of PPM treatment using an Olympus IX73 light microscope (Olympus Corporation). The experimental procedure and dosing treatment plan were presented in Fig. 2C, which was drawn using Figdraw (ID, RUUPO33f33; www.figdraw.com).

Mitochondrial membrane potential detection. The mitochondrial membrane potential was assessed using a JC-1 assay (cat. no. 10009172, Cayman Chemical Company). Briefly, cells were incubated with JC-1 staining solution (1:10) for 30 min at 37˚C. Subsequently, the cells were washed twice with assay

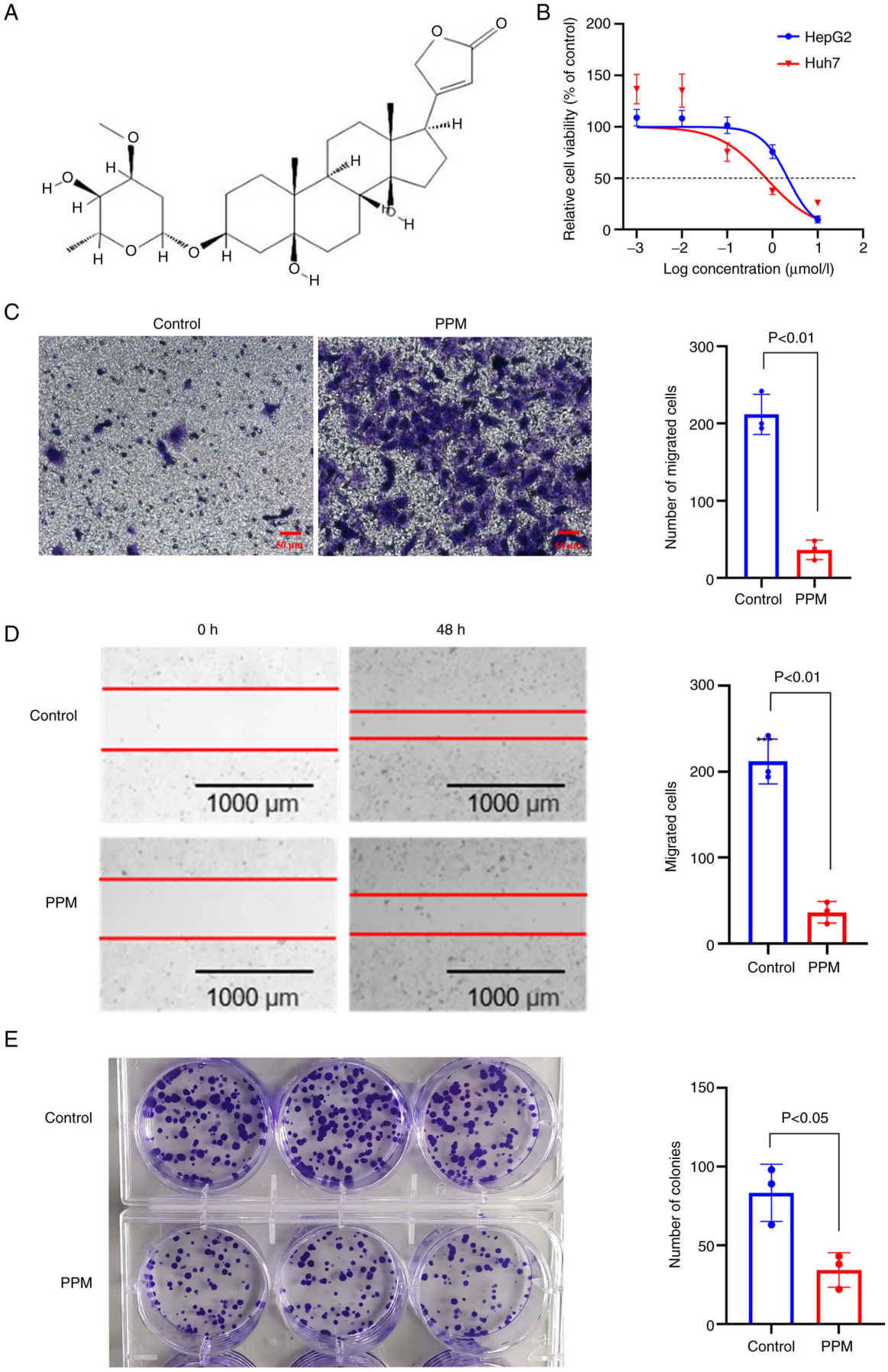

Figure 1. PPM inhibits the growth of liver cancer cells. (A) The chemical structure of PPM. (B) HepG2 and Huh7 cells were treated with different concentrations (1-10,000 nmol/l) of PPM for 48 h, and cell viability was measured using MTS assays. (C) Transwell invasion assays were used to assess HepG2 cell invasion ability. Scale bar=50 μm. (D) A scratch wound assay for HepG2 cells transfected with or without PPM. Scale bar=1,000 μm. (E) Colony formation assays for HepG2 cells transfected with or without PPM. Data are presented as mean ± SD, n=3. PPM, periplocymarin.

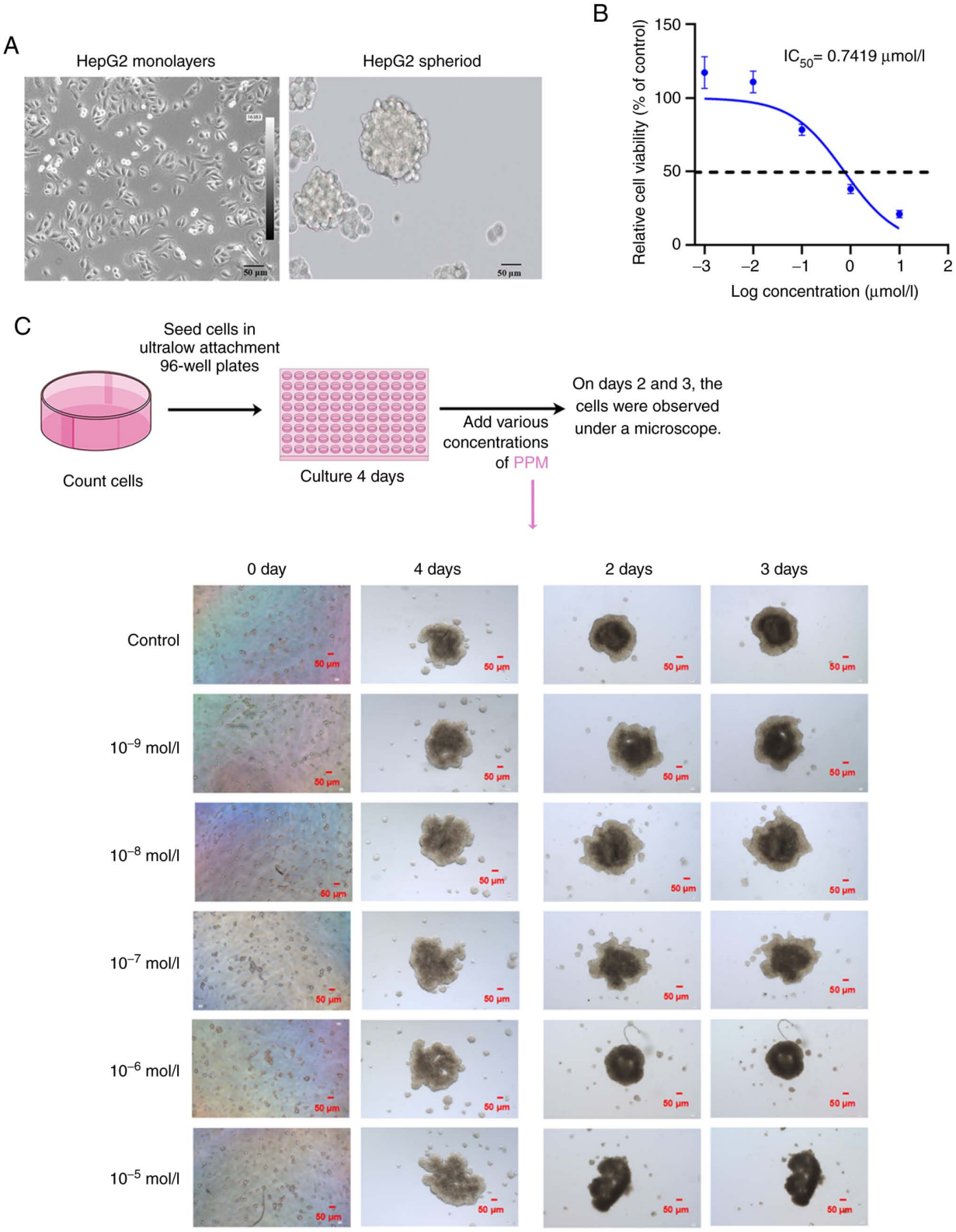

Figure 2. Establishing the 3D model from HepG2 cell lines. (A) Representative micrographs of HepG2 cells cultured in monolayer and spheroid. Scale bar=50 μm. (B) MTS assay was used to assess whether HepG2-3D cells treated with PPM were viable at 48 h. IC_{50}=0.7419 μmol/l. (C) The sphere-formation of HepG2 cells induced by PPM (10^{-5}, 10^{-6}, 10^{-7}, 10^{-8} and 10^{-9} mol/l) was tracked by microscopy. PPM, periplocymarin.

buffer to remove free JC-1 and immediately imaged using a fluorescence microscope.

Metabolic assay. HepG2 cells were cultured in Seahorse XF24 cell culture microplates (Agilent Technologies, Inc.) and cultured at 37˚C overnight. PPM (100 nmol/l) was added to the cells when they reached 80-90% confluence and cells were incubated for 24 h at 37˚C. This experiment was performed using the Seahorse XF Real-time ATP rate assay kit (cat. no. 103592-100; Agilent Technologies, Inc.). The

experimental procedures and Seahorse assays were performed according to the manufacturer's protocols. Wave software version 2.4.1 (Agilent XFp Analyzer; Agilent Technologies, Inc.) and GraphPad Prism version 9 (GraphPad Software.; Dotmatics) were used for statistical analysis and graphical representation.

Western blotting. HepG2 cells were treated with PPM in the presence or absence of 5 mM 3-methyladenine (3-MA, cat. no. HY-19312; MedChemExpress) (26), 50 nmol/l Bafilomycin A1 (Baf A1, cat. no. HY-100558; MedChemExpress) (27) or 20 μmol/l Z-VAD-FMK (cat. no. HY-16658B; MedChemExpress) (28) at 37˚C for 24 h. Total proteins were extracted from HepG2 cells using RIPA lysis buffer supplemented with Pierce Phosphatase Inhibitor (cat. no. A32961, Thermo Fisher Scientific, Inc.). The protein concentration was determined using a BCA kit (cat. no. 23227, Thermo Fisher Scientific, Inc.). SDS-PAGE was performed on 4-20% SDS-gels (GenScript), followed by transfer of the resolved proteins onto nitrocellulose membranes. Membranes were blocked in blocking buffer (cat. no. P0252, Beyotime Institute of Biotechnology) for 20 min at room temperature. Membraned were subsequently incubated with primary antibodies against anti-caspase 3 (1:1,000, cat. no. 14220, Cell Signaling Technology, Inc.); anti-pro-caspase-3, (1:1,000, cat. no. ab13847, Abcam) anti-caspase 7 (1:1,000, cat. no. ab32522, Abcam), anti-caspase 9 (1:1,000, cat. no. ab32539, Abcam), anti-Bcl-2 (1:1,000, cat. no. ab59348, Abcam), anti-Bax (1:1,000, cat. no. ab32503, Abcam), anti-α-tubulin (1:1,000, cat. no. ab7291, Abcam), anti-β-actin (1:1,000, cat. no. 3700, Cell Signaling Technology, Inc.), anti-microtubule-associated protein light chain 3 (LC3; 1:1,000, cat. no. ab192890, Abcam), anti-autophagy-related gene 4B (ATG4B; 1:1,000, cat. no ab154843, Abcam), anti-sequestosome 1/p62 (SQSTM1/p62; 1:1,000, cat. no. ab109012, Abcam), anti-GAPDH (1:1,000, cat. no. ab8245, Abcam), anti-phosphorylated-Unc-51-like kinase 1 (p-ULK1, ser757; 1:1,000, cat. no. 14202, Cell Signaling Technology, Inc.), anti-ULK1 (1:1,000, cat. no. 8054, Cell Signaling Technology, Inc.), anti-p-AMPKα (Thr172; 1:1,000, cat. no. 2535, Cell Signaling Technology, Inc.), anti-AMPKα (1:1,000, cat. no 5832, Cell Signaling Technology, Inc.), anti-p-mTOR (ser2481; 1:1,000, cat. no. 2974, Cell Signaling Technology, Inc.), anti-mTOR (1:1,000, cat. no. 2983, Cell Signaling Technology, Inc.), anti-lysosomal-associated membrane protein 1(LAMP1;1:1,000, cat. no. 21997-1-AP, Proteintech Group, Inc.), anti-cathepsin D (CTSD; 1:1,000, cat. no. 21327-1-AP, Proteintech Group, Inc.), or anti-cathepsin D (CTSB; 1:1,000, cat. no. 12216-1-AP, Proteintech Group, Inc.) overnight at 4˚C. After three rinses, the membrane was incubated with goat anti-mouse IgG H&L (IRDye® 680RD; 1:5,000, ab216776, Abcam) or goat anti-rabbit IgG H&L (IRDye® 800CW; 1:5,000, ab216773, Abcam) for 1 h at 37˚C. A LI-COR Odyssey CLx scanning system (LI-COR Biosciences) was used to semi-quantify the fluorescent signals, which were normalized to β-actin, GAPDH or α-tubulin expression as appropriate.

Red fluorescence point-green fluorescence point-LC3 (RFP-GFP-LC3) for determining autophagic flux. HepG2 cells were cultured to ~60% confluency. Autophagic flux was assessed using a Premo™ Autophagy Tandem Sensor RFP-GFP-LC3B Kit (cat. no. P36239, Thermo Fisher Scientific, Inc.) according to the manufacturer's protocols. Confocal images were acquired using a Carl Zeiss LSM710 confocal microscope (Zeiss GmbH).

Annexin V apoptosis assay. Apoptosis was assessed using a FITC Annexin V apoptosis detection kit (BD Biosciences). A total of $1x10^5$ HepG2 cells/well were seeded in 6-well plates and cultured at 37˚C for 24 h. After treatment with 100 nmol/l PPM for 24 h at 37˚C, the cells were resuspended in 100 μl binding buffer. Incubation was performed in the dark at room temperature for 15 min following the addition of 5 μl Annexin V-FITC and 10 μl PI. Finally, 400 μl PBS was added to each tube, and the cells were immediately evaluated by flow cytometry using a FACSAria™ III Cell Sorter (BD Biosciences). The percentage of apoptotic cells was calculated based on the number of apoptotic cells in each sample (Q2 + Q4).

Short interfering (si)RNA transfection. ATPase Na^+/K^+ Transporting Subunit α 1 (ATP1A1) siRNA and its negative control siRNA (cat. No. siN0000001-1-5) were purchased from Guangzhou RiboBio Co., Ltd. The sequences of the synthesized siRNA were as follows: si-ATP1A1-01, 5'-GATTCGAAATGGTGAGAAA-3'; si-ATP1A1-02, 5'-GTCGTCTGATCTTTGATAA-3'; and si-ATP1A1-03, 5'-GAATTTCCCTATCGATAAT-3'. Cells were seeded in 6-well plates at a density of $2x10^5$ cells/well. When the cells were 60% confluent, they were transfected with 50 nmol/l siRNA using the RiboFECT CP Transfection kit (Guangzhou RiboBio Co., Ltd.) according to the manufacturer's protocols. Subsequently, analysis of protein expression levels was performed in HepG2 cells after 24 h of treatment with PPM.

Assessment of membrane potential. HepG2 cells were placed in a recording chamber on the stage of an Olympus IX53 inverted microscope (Olympus Corporation). The experimental procedure was performed as previously described (29-31). Briefly, the extracellular solution (NaCl, 140 mmol/l; KCl, 4 mmol/l; $MgCl_2$, 1 mmol/l; $CaCl_2$, 2 mmol/l; D-glucose monohydrate, 5 mmol/l; 2-[4-(2-Hydroxyethyl) piperazin-1-yl] ethanesulfonic acid, 10 mmol/l; pH, 7.4) was continuously perfused into the recording chamber using a gravity-fed solution delivery system. The membrane potential was recorded in a whole-cell single-electrode current-clamp configuration using the patch-clamp technique with a 700 B amplifier (Molecular Devices, LLC). A computer equipped with a DigiData1550B (Molecular Devices, LLC) was used to generate the holding membrane current (I=0A) for data storage and evaluation. The patch electrodes had a resistance of 2-5 MΩ (P-97, Sutter Instrument Company) when filled with the internal solution (KCl, 20 mmol/l; $MgCl_2$, 1 mmol/l; Ethylenebis (oxyethylenenitrilo) tetraacetic acid, 5 mmol/l; phosphocreatine disodium salt, 14 mmol/l; Na_2-ATP, 5 mmol/l; pH, 7.2).

Electron microscopy. HepG2 cells were fixed in 2.5% glutaraldehyde in 0.1 M sodium cacodylate buffer at 4˚C for 2 h, followed by 1% osmium tetroxide in 0.1 M sodium cacodylate buffer for 2 h at room temperature. Then, they were stained

using 1% uranyl acetate for 1 h at room temperature, dehydrated in an increasing ethanol series and embedded in epoxy resin. The cells were subsequently imaged using a Hitachi-HT7700 electron microscope (Hitachi, Ltd.).

Xenograft mouse model. Animals were housed in appropriate pathogen-free conditions. All animal experiments (approval no. 2022023) adhered to the specifications of the Animal Care and Use Committee of Hebei Yiling Chinese Medicine Research Institute (Shijiazhuang, China). A total of 20 male BALB/c nude mice (5 weeks old, 18-22 g) were purchased from Beijing Vital River Laboratory Animal Technology Co., Ltd. (approval no. 110011220101738322). Mice were housed (n=5 per cage) in a rodent facility with a 12 h light/dark cycle, at 22˚C and 40% humidity, with *ad libitum* access to food and water. The 50% (v/v) Matrigel (cat. no 356234, Corning, Inc.)-suspended HepG2 cells ($2x10^6$/mouse) were injected subcutaneously into the flank of BALB/c nude mice. Tumor size was measured at day 14, and mice with a similar size tumor were selected for further experiments. When the tumor volume of the nude mice reached 200 mm^3, the mice were randomly divided into three groups of four mice each as follows: PPM (100 mg/kg), 3-MA (2 mg/kg) + PPM (100 mg/kg), and NaCl (control). The remaining 8 mice were excluded as the tumors did not reach 200 mm^3. Mice were treated daily via oral gavage for 7 days. Tumor diameter and mouse weight were measured every 3 days. The formula used to calculate the volume of the tumors was as follows: Volume=($width^2$ x length) x0.5. The experiments were terminated when tumor volumes reached ~1,500 mm^3. Pentobarbital sodium (50 mg/kg) was injected intraperitoneally into mice to anesthetize them (32). Tumor xenografts of each mouse were removed and weighed. After completion of the experiments, the mice were sedated with CO_2/O_2 (70%/30%). Once the mice lost consciousness, they were euthanized with 100% CO_2. The animals remained in the euthanasia chamber for 5 min and were then observed for an additional 5 min. Breathing and heart rate were monitored to determine death.

Immunofluorescence staining. For *in vivo* studies, tumor tissues were rapidly embedded with OCT embedding agent (cat. no. G6059, Wuhan Servicebio Technology Co., Ltd.) and snap-frozen on dry ice. Frozen sections were cut into 10-μm-thick slices. Ki67 is a cellular marker of proliferation (33) and the tumor cell proliferation rate was analyzed using Ki67 staining. Tunnel staining (cat. no. PF00006, ProteinTech Group, Inc.) was used to examine tumor cell apoptosis, according to the manufacturer's protocol.

For *in vitro* studies, HepG2 cells were seeded on 35 mm confocal dishes (Corning, Inc.) and cultured at 37˚C in 5% CO_2. After treatment with 100 nmol/l PPM for 24 h at 37˚C, HepG2 cells were fixed with 4% paraformaldehyde for 20 min at room temperature and then washed twice with PBS (5 min each). HepG2 cells were permeabilized with 0.5% Triton X-100 (cat. no. P0096, Beyotime Institute of Biotechnology) for 10 min at room temperature, and subsequently blocked in PBS with 10% goat serum (Beyotime Institute of Biotechnology) for 1 h at room temperature. SQSTM1/p62 and LC3 proteins are markers for autophagosome formation and degradation, respectively (34). HepG2 cells were subjected to immunofluorescence staining to assess LC3 and p62/SQSTM1 protein expression levels.

The primary antibodies used were as follows: Anti-Ki67 (1:250, cat. no. ab16667, Abcam), anti-LC3 (1 μg/ml, cat. no. ab192890, Abcam) or anti-SQSTM1/p62 (1 μg/ml, cat. no. ab109012, Abcam). Cells were incubated in primary antibodies overnight at 4˚C, washed with 1X PBS, and then incubated with fluorescently labeled secondary antibodies for 1 h in the dark at 37˚C. Secondary antibodies used were as follows: donkey anti-Rabbit Alexa Fluor 555 (1:1,000; cat. nos. P0179; Beyotime Institute of Biotechnology) and Alexa Fluor 488 goat anti-Rabbit (1:1,000; P0176; Beyotime Institute of Biotechnology). Each section was stained with DAPI (cat. no. S2110, Beijing Solarbio Science & Technology Co., Ltd.). for 1 h at room temperature and protected from light. Samples were imaged using a LSM710 confocal microscope (Zeiss GmbH) and analyzed using Image J (version 18.0; National Institutes of Health).

Statistical analysis. Data were presented as the mean ± standard deviation. Data was analyzed using one way analysis of variance with Tukey's post-hoc test. Statistical analysis was performed using SPSS version 19.0 (IBM Corp.). $P<0.05$ was considered to indicate a statistically significant difference.

Results

Effects of PPM in liver cancer cellular behaviors. To evaluate the biological effects of PPM in liver cancer, MTS assays were performed. The results demonstrated that PPM exhibited a cytotoxic effect on the HepG2 and Huh7 cells after 48 h of treatment with half-maximal inhibitory concentrations (IC_{50}) of 2.1860 and 0.7725 μmol/l, respectively (Fig. 1B). In the Transwell and wound healing assays, PPM significantly decreased the migratory ability of cells (Fig. 1C and D). The colony formation assays demonstrated that PPM significantly inhibited HepG2 colony formation (Fig. 1E). In the 3D cultures, HepG2 cells formed spheres with a grape-like appearance (Fig. 2A). Initially, the cells were diffusely distributed. With increasing culture times, the cell volume grew continuously and by day 4, cells appeared spherical or elliptical. After the administration of PPM, the structure of the cancer spheroids loosened within 48 h. These results demonstrated that PPM exhibited cytotoxic activity after 48 h on the cancer spheroids with an IC_{50} of 0.7419 μmol/l (Fig. 2B and C). PPM inhibited cell proliferation, migration and tumor sphere-formation ability. These data demonstrated that PPM exerted an anti-cancer effect in liver cancer cells *in vitro*.

PPM activates the mitochondrial apoptotic pathway in HepG2 cells. JC-1 is a critical marker of cell viability. Exposure of HepG2 cells to PPM markedly disrupted the mitochondrial membrane potential, based on the increase in green fluorescence (JC-1 monomers) and decrease in red fluorescence (JC-1 aggregates; Fig. 3A). CGs are known to exert their action primarily by binding to the α-subunit of the Na^+/K^+ATPase (NKA) pump and inhibiting the intake of K^+ coupled with the release of Na^+ out of the cell (35,36). As changes in intracellular ion concentrations can affect the resting membrane potential, the resting membrane potential of HepG2 cells treated

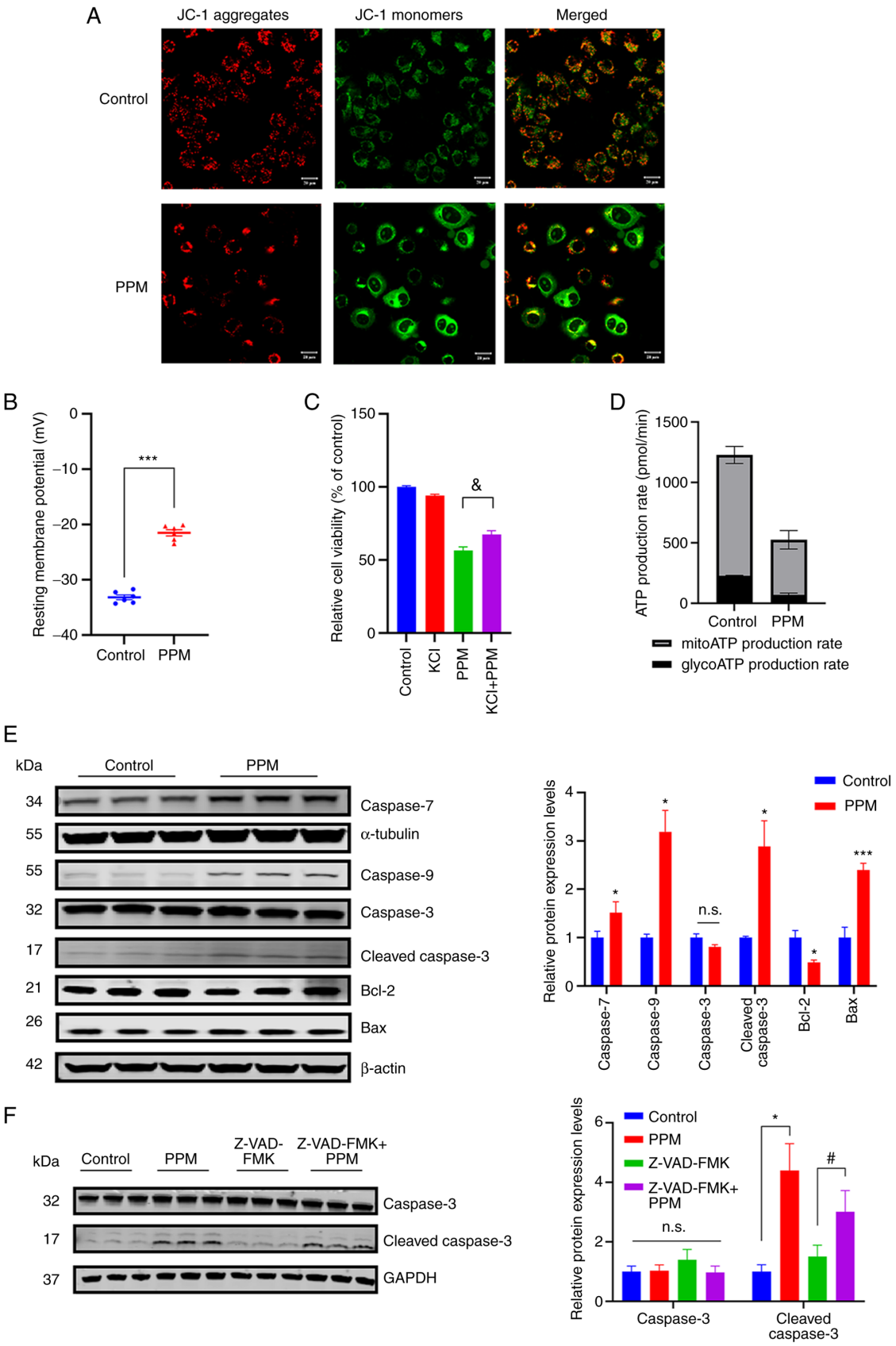

Figure 3. PPM activates the mitochondrial intrinsic apoptotic pathway. (A) Representative fluorescence microscopy images of JC-1 staining; red fluorescence represents the mitochondrial aggregate JC-1 and green fluorescence indicates the monomer JC-1. Scale bar=20 μm. (B) Resting membrane potential. (C) Relative cell viability of HepG2 cells treated with PPM and/or 25 mmol/l KCl for 24 h. (D) ATP production rates due to glycolysis or mitochondrial respiration as measured with the XF Real-Time ATP rate assay using XFe24 Agilent Seahorse. (E) The protein expression levels of caspase 7, caspase 9, caspase 3, cleaved caspase 3, Bcl-2 and Bax in HepG2 cells treated with PPM were assessed using western blotting. (F) HepG2 cells were treated with PPM (100 nmol/l) and/or 20 μmol/l Z-VAD-FMK for 24 h. Caspase 3 and Cleaved caspase 3 protein expression levels were assessed using western blotting. GAPDH was used as the loading control. Data are presented as mean ± SD, n=3; *P<0.05 and ***P<0.001 vs. control. $^{\&}$P<0.05 vs. KCl. $^{\#}$P<0.05 vs. Z-VAD-FMK. n.s., not significant. PPM, periplocymarin; glycolATP, glycolytic ATP; mitoATP, mitochondrial ATP.

with PPM was assessed. After treatment, PPM significantly depolarized the membrane potential in the PPM-treated cells (-21.5±1.37 mV) compared with the control (-33.2±1.05 mV; Fig. 3B). To alleviate depolarization of the plasma membrane, KCl was added to the medium (12). Addition of KCl restored cell viability independent of PPM inhibition (Fig. 3C). These results indicated that, plasma membrane depolarization was involved in the anticancer effects of PPM in liver cancer. PPM-treated HepG2 cells demonstrated lower ATP production from both the glycolytic and mitochondrial pathways (Fig. 3D). The protein expression levels of caspases following PPM treatment were assessed using western blotting. PPM significantly increased the protein expression levels of Bax, cleaved-caspase 3, caspase 9 and caspase 7 compared with the control, and significantly reduced the protein expression levels of Bcl-2 (Fig. 3E). To investigate the functional involvement of caspases in PPM-induced apoptosis, Z-VAD-FMK, an inhibitor of apoptosis, was used given its ability to function as a pan-caspase inhibitor. The results demonstrated that PPM significantly antagonized Z-VAD-FMK-induced inhibition of apoptosis (Fig. 3F). These results demonstrated that PPM activated the intrinsic mitochondrial apoptotic pathway.

PPM selectively activates macroautophagy via the AMPK/ULK1 and mTOR signaling pathways. LC3-II and p62/SQSTM1 are the most common markers of autophagy. The conversion of LC3-I into LC3-II serves as the gold standard for the detection of autophagy (37), and p62/SQSTM1, as an indicator of autophagic flow, links LC3-II with ubiquitinated substrates for degradation in autolysosomes (38,39). In the present study, the distribution of the intracellular autophagy marker LC3 was assessed to determine whether PPM could induce autophagy in HepG2 cells. The results demonstrated that PPM treatment significantly increased the accumulation of lipidated LC3 (conversion of LC3-I to LC3-II), which indicated the maturation of autophagosomes (Fig. 4A). AMPK is a known nutrient and energy sensor that maintains cellular energy homeostasis when the ratios of intracellular AMP/ATP levels are increased (40,41). AMPK is activated by phosphorylation at Thr172 (p-AMPK) (42). AMPK directly phosphorylates ULK1 at certain serine residues (S317, S555 and S777) to induce autophagy (43). To determine whether AMPK activation was involved in PPM-induced autophagy, the protein expression levels of p-AMPKα Thr172 and total AMPKα was assessed using western blotting. Protein expression levels of p-AMPKα (Thr1720 were significantly increased in HepG2 cells after PPM treatment compared with the control, whereas the total AMPKα expression was not significantly altered (Fig. 4B). Furthermore, PPM significantly reduced p-mTOR, p-ULK1 (ser 757) and total ULK1 protein expression levels compared with the control, whereas the total mTOR protein expression level was not significantly altered. Collectively, PPM activates macro-autophagy via the AMPK/ULK1 and mTOR pathways. To confirm the type of macro-autophagy, the protein expression levels of BNIP3 and PINK1, which are indicators of mitophagy activation, were assessed. PPM significantly decreased the protein expression levels of BNIP3 and PINK1 compared with the control (Fig. 4D). Notably, PPM treatment significantly increased the protein expression levels of p62/SQSTM1 and ATG4B compared with the control group (Fig. 4A), which was confirmed by immunofluorescence staining (Fig. 4C). Since simultaneously increased protein levels of p62/SQSTM1 and LC3-II indicated dysfunction of autophagy degradation (44), these findings suggested that PPM may have exerted differential effects at different stages of autophagy.

PPM activates macro-autophagy in an NKA receptor-dependent manner to counteract the pro-apoptosis effects. CGs work by inhibiting NKA and activating Na^+/Ca^{2+} exchange, which leads to an increase in the intracellular Ca^{2+} concentration (45). The inhibitory effect is produced by binding to the α-subunits of NKA (46). To confirm the activation of autophagy in an NKA-dependent manner, HepG2 cells were transfected with a set of three siRNAs, and ATP1A1 mRNA and protein expression levels were significantly reduced in the si-ATP1A1-02 group 48 h post-transfection, compared with the NC group (Fig. S1A and B). Furthermore, PPM did not significantly induce the protein expression of LC3-II in the ATP1A1 knockdown HepG2 cells (Fig. 5A). To evaluate the interactions between PPM-induced apoptosis and autophagy, HepG2 cells were treated with PPM in the presence or absence of 3-MA. The combination of 3-MA and PPM significantly inhibited the viability of HepG2 compared with PPM alone after 24 h, which suggested that blocking autophagy with 3-MA enhanced the cytotoxic effects of PPM on HepG2 cells (Fig. 5B). Flow cytometry analysis demonstrated that compared with the PPM group, the combined PPM and 3-MA treatment resulted in significantly increased apoptotic cell death (Fig. 5C).

The pro-apoptotic effects of PPM may impair the function of autophagic lysosomes. The protein expression levels of LC3-II were significantly increased in the combined treatment group compared with 3-MA alone; however, the 3-MA + PPM did not demonstrate a significant increase in LC3-II protein expression levels compared with PPM alone (P=0.55; Fig. 6A). Electron microscopy results demonstrated that a large number of autophagic lysosomes were present in the PPM group, which suggested that the degradation of autophagolysosomes may have been impaired in HepG2 cells (Fig. 6B). The autophagic degradation inhibitor, Baf A1 (50 nmol/l) was used to further assess how PPM regulated autophagic degradation. LC3-II protein expression levels were not markedly increased in the Baf A1 + PPM group compared with that in the Baf A1 group, which demonstrated that PPM intrinsically blocked autophagosome degradation (Fig. 6C). Furthermore, autophagic flux was directly monitored using the chimeric autophagic flux reporter protein RFP-GFP-LC3. PPM markedly increased yellow punctate fluorescence in HepG2 cells, which suggested an impairment of autophagosome-lysosome fusion. (Fig 6D). Subsequently, lysosomal function was evaluated in PPM-treated HepG2 cells by assessing the protein expression levels of CTSB, CTSD and LAMP1 (14). PPM significantly upregulated the expression of LAMP1 compared with the control and significantly downregulated the protein expression levels of CTSB and CTSD compared with the control, which indicated that PPM impaired lysosomal function by inhibition of proteolytic enzyme activity (Fig. 6E). To further investigate whether PPM-induced apoptosis was implicated in

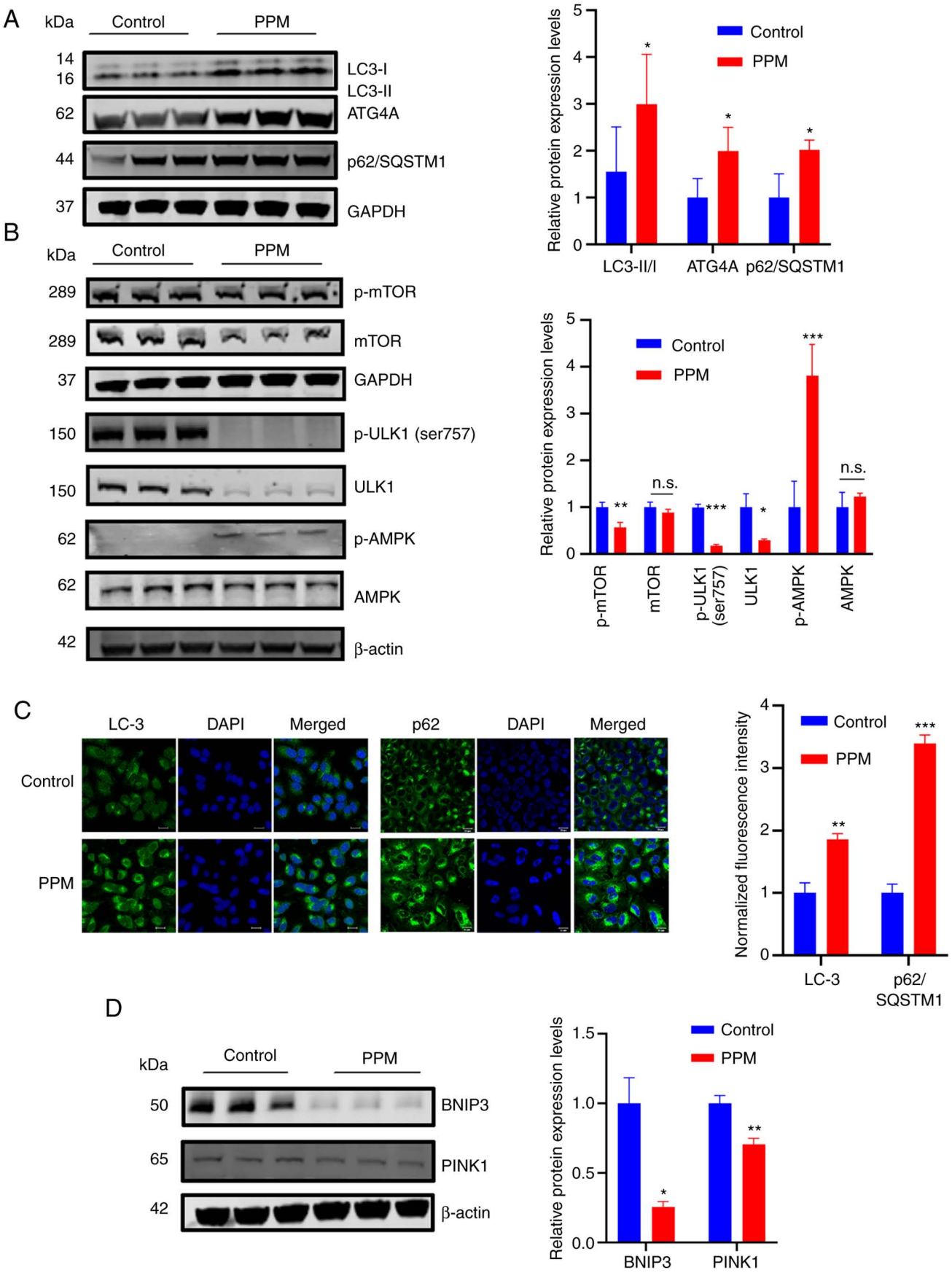

Figure 4. PPM selectively activated macroautophagy in HepG2 cells. (A) Western blotting of LC3, ATG4A and p62/SQSTM1 and (B) p-mTOR, mTOR, p-ULK1(Ser757), ULK1, p-AMPKα (Thr172) and AMPKα protein expression levels after treatment with PPM (100 nmol/l) in HepG2 cells. (C) Immunofluorescence staining of LC3 and p62/SQSTM1. Scale bar=20 μm. (D) Western blotting of the mitophagy markers BNIP3 and PINK1. GAPDH or β-actin was used as a loading control. Data are presented as mean ± SD, n=3; *P<0.05, **P<0.01 and ***P<0.001 vs. control. n.s., not significant; PPM, periplocymarin; p, phosphorylated; LC3, microtubule-associated protein light chain 3; ATG4A, ATG4A; p62/SQSTM1, sequestosome 1; ULK1, Unc-51-like kinase 1; BNIP3, BCL2 Interacting Protein 3; PINK1, PTEN induced putative kinase 1.

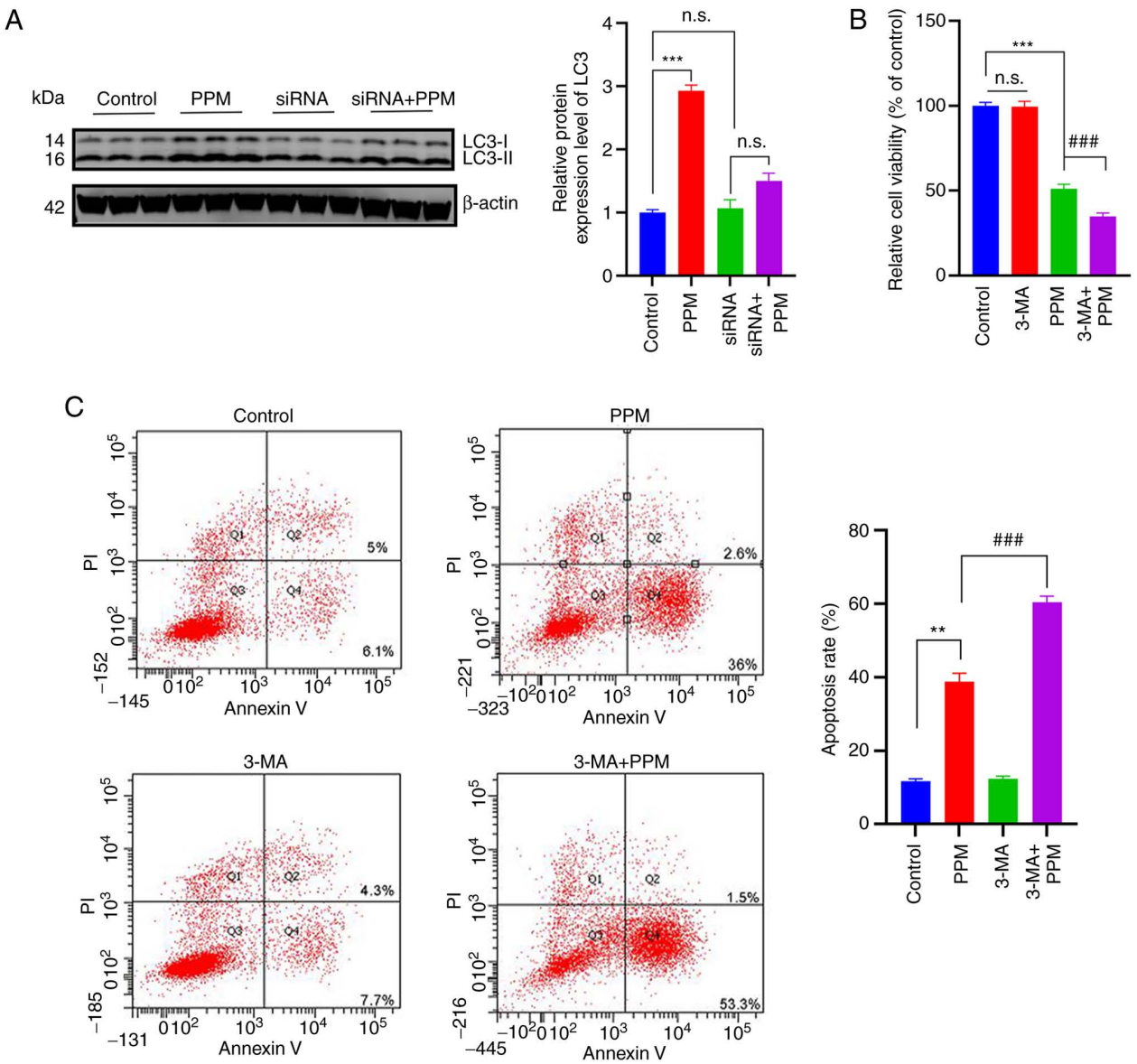

Figure 5. PPM-induced macroautophagy counteracted the apoptosis cell death. (A) LC3 protein expression levels of HepG2 cells with ATP1A1 knockdown and/or treated with PPM (100 nmol/l). HepG2 cells were treated with PPM (100 nmol/l) and/or 3-MA (5 mmol/l) for 24 h; (B) cell viability was then determined using MTS assays and (C) apoptosis was analyzed using flow cytometry. GAPDH or β-actin was used as a loading control. Data are presented as mean ± SD, n=3; **P<0.01 and ***P<0.001 vs. control. $^{###}$P<0.001 vs. PPM. n.s., not significant; PPM, periplocymarin; siRNA, short interfering; LC3, microtubule-associated protein light chain 3; ATP1A1, ATPase Na^+/K^+ transporting subunit α1.

the dysfunction of autophagy degradation, HepG2 cells were treated with PPM (100 nmol/l) alone or in combination with Z-VAD-FMK (20 μmol/l). The results demonstrated that PPM combined with Z-VAD-FMK significantly reduced the protein expression levels of LC3-II and p62/SQSTM1 compared with PPM alone (Fig. 6F).

PPM suppresses tumor growth in vivo. The therapeutic effect of PPM alone or in combination with 3-MA in HepG2 cells xenografts implanted into nude mice was evaluated. Combined treatment with PPM and 3-MA was significantly more effective in inhibiting tumor growth than PPM alone (Fig. 7A-D). Furthermore, the anti-proliferative and pro-apoptotic effects were assayed by immunofluorescence staining for Ki67 as well as by using Tunnel staining. PPM alone or in combination with 3-MA significantly increased the levels of apoptosis in tumor tissues compared with the control group (Fig. 7E). However, the protein expression level of Ki-67 in the control group was significantly greater than that in the PPM alone or PPM combined with 3-MA groups. Consistently, a reduction in Ki67 staining in the combination treatment group was significantly greater than that in the PPM group.

This demonstrated that PPM synchronously activated the lethal apoptosis and the protective autophagy in liver cancer, and that the autophagy counteracted the inherent pro-apoptosis capacities and impaired the anti-cancer effects.

Discussion

Over the last decades, the emerging roles of the NKA in a variety of critical cellular processes have indicated that NKA inhibitors, including CGs, may have potential novel therapeutic

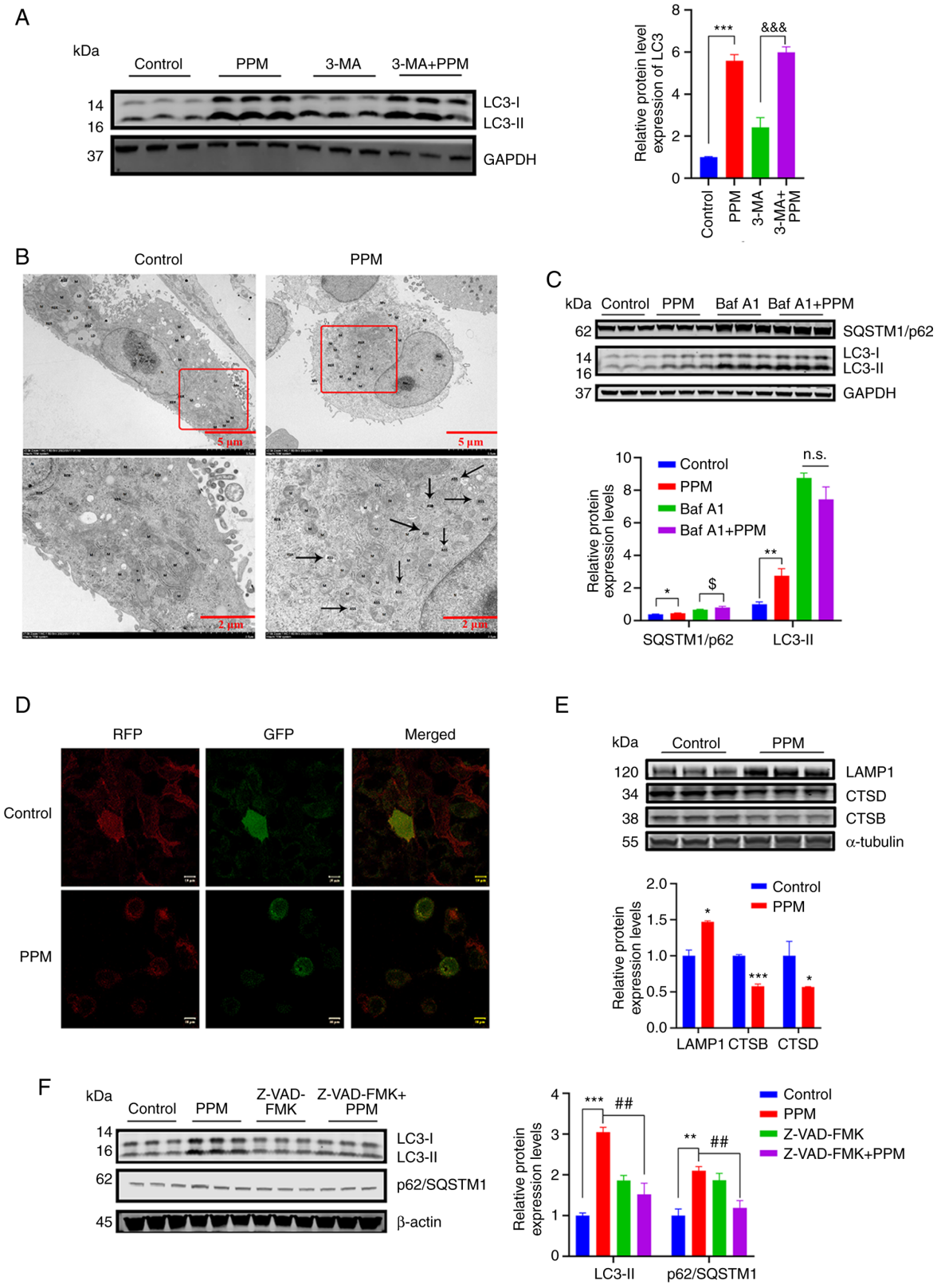

Figure 6. The pro-apoptosis effect of PPM might impair the function of autophagic lysosomes. (A) LC3 were assessed using western blotting. (B) Electron microscopy showed that PPM treatment led to autolysosome increase. Black arrows indicate the autolysosomes. (C) HepG2 cells were treated with PPM (100 nmol/l) and/or Baf A1 (50 nmol/l) for 24 h. LC3-II and p62/SQSTM1 protein expression levels were assessed using western blotting. (D) HepG2 cells were transfected with RFP-GFP-LC3 lentivirus and treated with PPM (100 nmol/l) for 24 h. Cells were observed to distinguish between autophagosome (yellow puncta) after colocalization analysis using a confocal microscope. Scale bar=10 μm. (E) HepG2 cells were treated with PPM (100 nmol/l) for 24 h and the protein expression levels of LAMP1, CTSB and CTSD were assessed using western blotting. (F) HepG2 cells were treated with PPM (100 nM) and/or 20 μmol/l Z-VAD-FMK for 24 h. LC3 and p62/SQSTM1 levels were detected by using western blot analysis. GAPDH or β-actin were used as a loading control. Data are presented as mean ± SD, n=3; *P<0.05, **P<0.01 and ***P<0.001 vs. control. $^{\&\&\&}$P<0.001 vs. 3-MA. $^{\$}$P<0.05 vs. Baf A1. $^{\#\#}$P<0.01 vs. PPM. n.s., not significant; ASS, autophagolysosome; M, mitochondria; PPM, periplocymarin; LC3, microtubule-associated protein light chain 3; SQSTM1/p62, sequestosome 1/p62; LAMP1, Lysosomal-associated membrane protein 1; CTSB, cathepsin B; CTSD, cathepsin D; RFP-GFP-LC3, red fluorescence point-green fluorescence point-LC3.

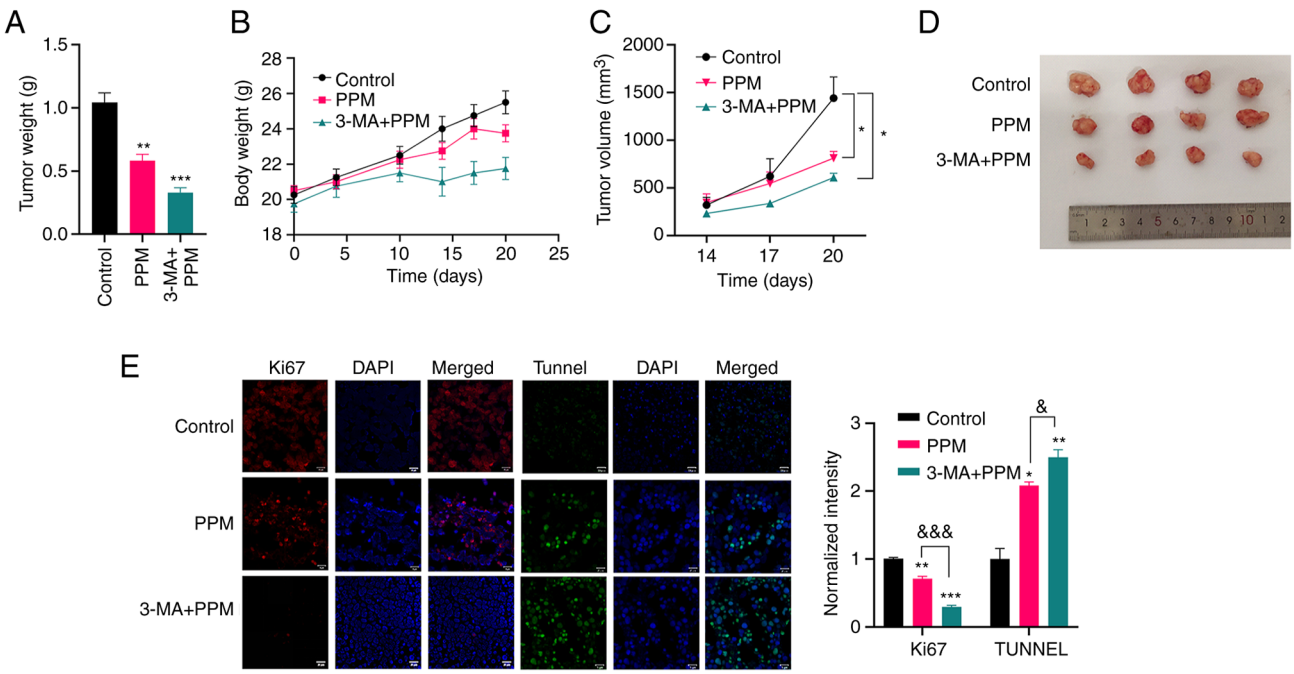

Figure 7. PPM exerted anti-tumor activity in the HepG2 xenograft tumor model. HepG2 xenograft tumors grew in nude mice after control (vehicle), PPM (100 mg/kg) and 3-MA (2 mg/kg) + PPM treatments administered orally daily for 7 days, n=4. (A) Average final tumor weight and (B) body weight of mice. (C) The growth of HepG2 xenograft tumors in nude mice. (D) Representative images of the tumor samples from each group. (E) Immunofluorescence staining for Ki67 and Tunnel in tumor sections. Scale bar=20 μm. Data are presented as mean ± SD. *P<0.05, **P<0.01 and ***P<0.001 vs. control; $^{\&}$P<0.05 and $^{\&\&\&}$P<0.001 vs. PPM. n.s., not significant; PPM, periplocymarin; 3-MA, 3-methyladenine.

purposes in diseases other than heart failure (14). Notably, compelling evidence has shown the anticancer properties of CGs in certain types of cancers and this has highlighted their potential use in cancer therapy. Although the anticancer effects of CGs alone or in combination with other drugs have been verified in both preclinical studies and clinical trials (47), the MOA of CGs remains unclear. Early studies suggested that the increased susceptibility of tumor cells to these CGs is dependent on the activation of apoptosis (48,49). CGs induce cell apoptosis by increasing the concentration of intracellular free calcium and induce S phase cell cycle arrest by down-regulating the expression of Cyclin A and CDK2 (50). CGs have been reported to have downregulated the expression of the anti-apoptotic protein Bcl-2 and increased the translocation of proapoptotic protein cytochrome C, which induced apoptosis (51). Durmaz *et al* (52) reported that CGs, particularly Lanatoside C could significantly inhibit, PTEN protein adequate, Huh7 and, PTEN deficient, Mahlavu human liver cancer cell proliferation by the induction of apoptosis and G2/M arrest in the cells. As NKA has been extensively studied as a potential anticancer target, CG-based NKA inhibitors have also been extensively studied, and apoptosis-independent death effects have been reported, including the involvement of the interferon signaling pathway, endogenous interactions of volume-regulated anion channels, activation of cancer-specific immune responses and inhibition of protective autophagy (53).

In the present study, the roles and mechanisms involved in the integrated regulation of macroautophagy and apoptosis in response to PPM was assessed in HepG2 cells. To avoid the selectivity of liver cancer cells, *in vitro* proliferation inhibition was performed in Huh7 and HepG2 cells and demonstrated IC_{50} values of 2.1860 μmol/l for Huh7 and 0.7725 μmol/l for HepG2 after an incubation time of 48 h. These findings demonstrated for the first time, to the best of our knowledge, that PPM exerted dual targeting of apoptosis and autophagy. To evaluate the interaction between apoptosis and protective autophagy *in vitro*, mutual antagonism between apoptosis and autophagy in PPM-treated HepG2 cells was evaluated. Briefly, macroautophagy induced by PPM counteracted apoptotic cell death; in turn, autophagic degradation activity was impaired by pro-apoptotic effects. Finally, the synergistic effect of the combined application of PPM and an autophagy inhibitor in BALB/c nude mice bearing HepG2 xenografts was demonstrated.

Although research on PPM for the treatment of liver cancer has not been previously reported, the increased susceptibility of other cancer cells to PPM has been reported, and induction of apoptosis is a common outcome (10,54), highlighting PPM as an organic potential anticancer agent (16). The present study demonstrated the anticancer effects of PPM through the inhibition of proliferation, migration, and clonal and spheroid formation in HepG2 cells. A pro-apoptotic programmed cell death (PCD) pattern was evaluated, which demonstrated that PPM treatment resulted in an elevated membrane potential of the mitochondria and impaired mitochondrial functions, including reduced ATP production, which indicated that the mitochondria-mediated intrinsic apoptotic pathway was concomitantly activated. To validate the pro-apoptotic MOA of PPM, Z-VAD-FMK, a specific apoptosis inhibitor, was used, which reversed the pro-apoptotic effect of PPM by significantly reducing the protein expression level of cleaved caspase-3.

Research has suggested that high levels of autophagy also result in increased cell death (55). The unique form of autophagy-dependent cell death is termed 'autosis' (56),

which is mediated by NKA and is characterized by numerous autophagosomes/autolysosomes and nuclear convolution during the early stages, and by dismantling of cellular organelles and focal ballooning of the perinuclear space in the later stages (57). CGs have been shown to induce autophagy in certain cancer types (47). To investigate whether autophagic processes could be triggered by PPM to inhibit autosis or autophagic cell death (58), the expression of autophagy-related genes was assessed. Inconsistent with previous studies on the inhibition of autosis, the present study demonstrated that PPM significantly increased LC3-II protein expression levels, which in-turn activated macroautophagy via the AMPK/ULK1 and mTOR signaling pathways. Moreover, the decreased expression of BNIP3 and PINK1, biomarkers of mitophagy, demonstrated that PPM selectively induced macroautophagy activation. How these changes in autophagy-related genes enhanced the anti-cancer susceptibility to PPM requires future study. Inhibition of autophagy by 3-MA increased the pro-apoptotic effects of PPM in HepG2 cells, which supported the evidence that autophagy and apoptosis serve opposing roles in tumor cells (55). These data indicated that inhibition of autophagy sensitized HepG2 cells to PPM-induced apoptosis. However, when the increased p62/SQSTM1 protein expression levels were assessed, new problems emerged: Autophagic degradation may be impaired, and it may have been that the activated apoptosis counteracted this degradation process.

The mechanisms linking autophagy and apoptosis have not been fully delineated (59). In the present study, the activation of autophagy elevated the threshold of PPM-mediated apoptosis. To evaluate whether PPM-mediated autophagy was a compensatory response, knockdown of ATP1A1 (the NKA gene) by siRNA mostly inhibited the expression of LC3-II in HepG2 cells treated with PPM, which indicated that protective autophagy was triggered by PPM by direct targeting of NKA. Electron microscopy demonstrated the accumulation of autophagosomes/autolysosomes in PPM-treated cells. Since the accumulation of autophagosomes/autolysosomes manifests as blockage of autophagic degradation, we examined the effect of PPM on autophagy flux and activity by combining PPM with Baf A1, an autophagic degradation inhibitor. Compared with Baf A1 alone, PPM combined with Baf A1 did not significantly increase the conversion of LC3-I to LC3-II, which indicated that PPM is an autophagic degradation inhibitor. Consistent with these results, it was demonstrated that PPM increased the number of yellow puncta in the RFP-GFP-LC3 fluorescence assay, which suggested that autophagic degradation was blocked in HepG2 cells treated with PPM. Taken together, these results indicated that PPM may interfere with the fusion of autophagosomes and lysosomes. The decreased protein expression levels of CTSD and CTSB demonstrated that PPM affected the metabolic degradation of lysosomes to block autophagic flux in HepG2 cells, and the protein expression level of LAMP1 was assessed to exclude the possibility of direct damage to lysosomes by PPM. The present study demonstrated that PPM simultaneously activated lethal apoptosis and protective autophagy in HepG2 cells. Next, whether the activation of apoptosis counteracted the autophagy degradation process was assessed. The apoptosis inhibitor, Z-VAD-FMK, combined with PPM significantly inhibited the protein accumulation of LC3-II and p62/SQSTM1, which indicated that the apoptosis induced by PPM was implicated in decreased autophagy degradation. Since several clinical trials for CGs in cancer are currently underway, their real-world benefits in liver cancer patients and their potential self-limiting effects *in vitro* remain uncertain. To validate the anti-cancer effects of PPM *in vivo* and the hypothesis that a combination of an autophagy inhibitor may be an improved strategy for the treatment of PPM in liver cancer, nude mice were used to establish xenograft models and it was demonstrated that the tumor volume and weight in the combination treatment group were significantly smaller than those in either of the single-agent treatment groups. Furthermore, immunofluorescence studies for Ki67 demonstrated a marked reduction in proliferation in the tissues from the mice treated with the combination of drugs, which further indicated the regression of tumors in the mouse models.

In conclusion, the results demonstrated that PPM, a CG, exerts an anti-cancer effect by inducing apoptosis; that PPM-induced autophagy activation occurred in an NKA receptor-dependent manner and counteracted, to some extent, the pro-apoptotic effect of PPM, and vice versa; that the abrogation of autophagic flux resulted from decreased protein levels in the lysosomes; and the combined application of PPM with an autophagy inhibitor may be a good option to enhance the pro-apoptotic activity of PPM *in vitro* and the anti-tumor activity *in vivo*. A limitation of the present study was the small number of animals included, which may need to be enlarged in future investigations.

These results provide novel insights into the MOA of PPM, and indicate PPM as a potential therapeutic agent against liver cancer, whilst also showing activation of protective autophagy by PPM. Finally, an improved strategy, consisting of a combination of PPM and autophagy inhibitors, was assessed and this showed improved anti-tumor effects.

Acknowledgments

Not applicable.

Funding

This research was supported by the HaiYan Fund of Harbin Medical University Cancer Hospital (grant no. JJMS2021-16), Research project of China Primary Health Care Foundation (grant no. 2022-001) and S&T Program of Hebei (grant no. E2020100001).

Availability of data and materials

The datasets used and/or analyzed during the current study are available from the corresponding author on reasonable request.

Authors' contributions

YHo and HH designed the study. YHa completed the first draft of this manuscript. YHa, TS and MW performed the experiments. ToL, CZ and TiL analyzed the data and revised the manuscript. YHa, TS and YHo confirm the authenticity of all the raw data. All authors have read and approved the final version of the manuscript.

Ethics approval and consent to participate

The study was approved by the Animal Care and Use Committee of Hebei Yiling Chinese Medicine Research Institute (approval no. 2022023).

Patient consent for publication

Not applicable.

Competing interests

The authors declare that they have no competing interests.

References

1. Bray F, Ferlay J, Soerjomataram I, Siegel RL, Torre LA and Jemal A: Global cancer statistics 2018: GLOBOCAN estimates of incidence and mortality worldwide for 36 cancers in 185 countries. CA Cancer J Clin 68: 394-424, 2018.
2. Massarweh NN and El-Serag HB: Epidemiology of hepatocellular carcinoma and intrahepatic cholangiocarcinoma. Cancer Control 24: 1073274817729245, 2017.
3. Bruix J, Gores GJ and Mazzaferro V: Hepatocellular carcinoma: Clinical frontiers and perspectives. Gut 63: 844-855, 2014.
4. Guo H, Wu T, Lu Q, Li M, Guo JY, Shen Y, Wu Z, Nan KJ, Lv Y and Zhang XF: Surgical resection improves long-term survival of patients with hepatocellular carcinoma across different Barcelona clinic liver cancer stages. Cancer Manag Res 10: 361-369, 2018.
5. Cheng L, Wang C, Ma X, Wang Q, Cheng Y, Wang H, Li Y and Liu Z: Multifunctional upconversion nanoparticles for dual-modal imaging-guided stem cell therapy under remote magnetic control. Advanced Functional Materials 21: 272-280, 2013.
6. Huang M, Shen S, Luo C and Ren Y: Genus periploca (Apocynaceae): A review of its classification, phytochemistry, biological activities and toxicology. Molecules 24: 2749, 2019.
7. Xie G, Sun L, Li Y, Chen B and Wang C: Periplocin inhibits the growth of pancreatic cancer by inducing apoptosis via AMPK-mTOR signaling. Cancer Med 10: 325-336, 2021.
8. Yun W, Qian L, Cheng Y, Tao W, Yuan R and Xu H: Periplocymarin plays an efficacious cardiotonic role via promoting calcium influx. Front Pharmacol 11: 1292, 2020.
9. Yun W, Qian L, Yuan R and Xu H: Periplocymarin alleviates doxorubicin-induced heart failure and excessive accumulation of ceramides. Front Cardiovasc Med 8: 732554, 2021.
10. Bloise E, Braca A, De Tommasi N and Belisario MA: Pro-apoptotic and cytostatic activity of naturally occurring cardenolides. Cancer Chemother Pharmacol 64: 793-802, 2009.
11. Li Y, Li J, Zhou K, He J, Cao J, An M and ChangYX: A review on phytochemistry and pharmacology of cortex periplocae. Molecules 21: 1702, 2016.
12. Triana-Martínez F, Picallos-Rabina P, Da Silva-Álvarez S, Pietrocola F, Llanos S, Rodilla V, Soprano E, Pedrosa P, Ferreirós A, Barradas M, *et al*: Identification and characterization of cardiac glycosides as senolytic compounds. Nat Commun 10: 4731, 2019.
13. Guerrero A, Herranz N, Sun B, Wagner V, Gallage S, Guiho R, Wolter K, Pombo J, Irvine EE, Innes AJ, *et al*: Cardiac glycosides are broad-spectrum senolytics. Nat Metab 1: 1074-1088, 2019.
14. Prassas I and Diamandis EP: Novel therapeutic applications of cardiac glycosides. Nat Rev Drug Discov 7: 926-935, 2008.
15. Kumavath R, Paul S, Pavithran H, Paul MK, Ghosh P, Barh D and Azevedo V: Emergence of cardiac glycosides as potential drugs: Current and future scope for cancer therapeutics. Biomolecules 11: 1275, 2021.
16. Martey ON, He X, Xing H, Deng F, Feng S, Li C and Shi X: Periplocymarin is a potential natural compound for drug development: Highly permeable with absence of P-glycoprotein efflux and cytochrome P450 inhibitions. Biopharm Drug Dispos 35: 195-206, 2014.
17. Zhao LM, Li L, Huang Y, Han LJ, Li D, Huo BJ, Dai SL, Xu LY, Zhan Q and Shan BE: Antitumor effect of periplocin in TRAIL-resistant gastric cancer cells via upregulation of death receptor through activating ERK1/2-EGR1 pathway. Mol Carcinog 58: 1033-1045, 2019.
18. Lohberger B, Wagner S, Wohlmuther J, Kaltenegger H, Stuendl N, Leithner A, Rinner B, Kunert O, Bauer R and Kretschmer N: Periplocin, the most anti-proliferative constituent of Periploca sepium, specifically kills liposarcoma cells by death receptor mediated apoptosis. Phytomedicine 51: 162-170, 2018.
19. White E, Mehnert JM and Chan CS: Autophagy, metabolism, and cancer. Clin Cancer Res 21: 5037-5046, 2015.
20. Schwartz LM: Autophagic cell death during development-ancient and mysterious. Front Cell Dev Biol 9: 656370, 2021.
21. Lockshin RA and Zakeri Z: Apoptosis, autophagy, and more. Int J Biochem Cell Biol 36: 2405-2419, 2004.
22. Levine B and Yuan J: Autophagy in cell death: An innocent convict? J Clin Invest 115: 2679-2688, 2005.
23. Trenti A, Grumati P, Cusinato F, Orso G, Bonaldo P and Trevisi L: Cardiac glycoside ouabain induces autophagic cell death in non-small cell lung cancer cells via a JNK-dependent decrease of Bcl-2. Biochem Pharmacol 89: 197-209, 2014.
24. Newman RA, Kondo Y, Yokoyama T, Dixon S, Cartwright C, Chan D, Johansen M and Yang P: Autophagic cell death of human pancreatic tumor cells mediated by oleandrin, a lipid-soluble cardiac glycoside. Integr Cancer Ther 6: 354-364, 2007.
25. Mariño G, Niso-Santano M, Baehrecke EH and Kroemer G: Self-consumption: The interplay of autophagy and apoptosis. Nat Rev Mol Cell Biol 15: 81-94, 2014.
26. Wang X, Zhou G, Liu C, Wei R, Zhu S, Xu Y, Wu M and Miao Q: Acanthopanax versus 3-methyladenine ameliorates sodium taurocholate-induced severe acute pancreatitis by inhibiting the autophagic pathway in rats. Mediators Inflamm 2016: 8369704, 2016.
27. Yang J, Wang B, Xu Q, Yang Y, Hou L, Yin K, Guo Q, Hua Y, Zhang L, Li Y, *et al*: TMEM166 inhibits cell proliferation, migration and invasion in hepatocellular carcinoma via upregulating TP53. Mol Cell Biochem 476: 1151-1163, 2021.
28. Liu HR, Peng XD, He HB, Wang YH, Li Y, He GX, Liu YL, Li YL and Zeng CJ: Antiproliferative activity of the total saponin of Solanum lyratum Thunb in Hela cells by inducing apoptosis. Pharmazie 63: 836-842, 2008.
29. Hyllienmark L and Brismar T: Effect of metabolic inhibition on K+ channels in pyramidal cells of the hippocampal CA1 region in rat brain slices. J Physiol 496: 155-164, 1996.
30. Hyllienmark L and Brismar T: Effect of hypoxia on membrane potential and resting conductance in rat hippocampal neurons. Neuroscience 91: 511-517, 1999.
31. Lin Z, Xing W, Gao C, Wang X, Qi D, Dai G, Zhao W and Yan G: Inhibitory effect of vascular endothelial growth factor on the slowly activating delayed rectifier potassium current in guinea pig ventricular myocytes. J Am Heart Assoc 7: e007730, 2018.
32. Zhang D, Gao JL, Zhao CY, Wang DN, Xing XS, Hou XY, Wang SS, Liu Q and Luo Y: Cyclin G2 promotes the formation of smooth muscle cells derived foam cells in atherosclerosis via PP2A/NF-κB/LOX-1 pathway. Ann Transl Med 9: 446, 2021.
33. Scholzen T and Gerdes J: The Ki-67 protein: From the known and the unknown. J Cell Physiol 182: 311-322, 2000.
34. Li X, Zhou Y, Zhang X, Cao X, Wu C and Guo P: Cordycepin stimulates autophagy in macrophages and prevents atherosclerotic plaque formation in ApoE(-/-) mice. Oncotarget 8: 94726-94737, 2017.
35. Medina-Ortiz K, López-Alvarez D, Navia F, Hansen T, Fierro L and Castaño S: Identification of Na(+)/K(+)-ATPase α/β isoforms in Rhinella marina tissues by RNAseq and a molecular docking approach at the protein level to evaluate α isoform affinities for bufadienolides. Comp Biochem Physiol A Mol Integr Physiol 254: 110906, 2021.
36. Bers DM: Cardiac excitation-contraction coupling. Nature 415: 198-205, 2002.
37. Liao YX, Yu HY, Lv JY, Cai YR, Liu F, He ZM and He SS: Targeting autophagy is a promising therapeutic strategy to overcome chemoresistance and reduce metastasis in osteosarcoma. Int J Oncol 55: 1213-1222, 2019.
38. Zhang XJ, Chen S, Huang KX and Le WD: Why should autophagic flux be assessed? Acta Pharmacol Sin 34: 595-599, 2013.
39. Seranova E, Ward C, Chipara M, Rosenstock TR and Sarkar S: In vitro screening platforms for identifying autophagy modulators in mammalian cells. Methods Mol Biol 1880: 389-428, 2019.
40. López M and Diéguez C: Cellular energy sensors: AMPK and beyond. Mol Cell Endocrinol 397: 1-3, 2014.
41. Timm KN and Tyler DJ: The role of AMPK activation for cardioprotection in doxorubicin-induced cardiotoxicity. Cardiovasc Drugs Ther 34: 255-269, 2020.

42. Hardie DG, Ross FA and Hawley SA: AMPK: A nutrient and energy sensor that maintains energy homeostasis. Nat Rev Mol Cell Biol 13: 251-262, 2012.
43. Kang SA, Pacold ME, Cervantes CL, Lim D, Lou HJ, Ottina K, Gray NS, Turk BE, Yaffe MB and Sabatini DM: mTORC1 phosphorylation sites encode their sensitivity to starvation and rapamycin. Science 341: 1236566, 2013.
44. Dyshlovoy SA: Blue-print autophagy in 2020: A critical review. Mar Drugs 18: 482, 2020.
45. Fozzard HA and Sheets MF: Cellular mechanism of action of cardiac glycosides. J Am Coll Cardiol 5: 10A-15A, 1985.
46. Mijatovic T, Quaquebeke V, Delest B, Debeir O, Darro F and Kiss R: Cardiotonic steroids on the road to anti-cancer therapy. Biochim Biophys Acta 1776: 32-57, 2007.
47. Škubník J, Pavlíčková VS, Psotová J and Rimpelová S: Cardiac glycosides as autophagy modulators. Cells 10: 3341, 2021.
48. Cheng CF, Lu IH, Tseng HW, Sun CY, Lin LT, Kuo ZK, Pan IH and Ko CH: Antitumor effect of periplocin in TRAIL-resistant human hepatocellular carcinoma cells through downregulation of IAPs. Evid Based Complement Alternat Med 2013: 958025, 2013.
49. Chao MW, Chen TH, Huang HL, Chang YW, HuangFu WC, Lee YC, Teng CM and Pan SL: Lanatoside C, a cardiac glycoside, acts through protein kinase Cδ to cause apoptosis of human hepatocellular carcinoma cells. Sci Rep 7: 46134, 2017.
50. Xu ZW, Wang FM, Gao MJ, Chen XY, Shan NN, Cheng SX, Mai X, Zala GH, Hu WL and Xu RC: Cardiotonic steroids attenuate ERK phosphorylation and generate cell cycle arrest to block human hepatoma cell growth. J Steroid Biochem Mol Biol 125: 181-191, 2011.
51. Rasheduzzaman M, Yin H and Park SY: Cardiac glycoside sensitized hepatocellular carcinoma cells to TRAIL via ROS generation, p38MAPK, mitochondrial transition, and autophagy mediation. Mol Carcinog 58: 2040-2051, 2019.
52. Durmaz I, Guven EB, Ersahin T, Ozturk M, Calis I and Cetin-Atalay R: Liver cancer cells are sensitive to Lanatoside C induced cell death independent of their PTEN status. Phytomedicine 23: 42-51, 2016.
53. Fujii T, Shimizu T, Yamamoto S, Funayama K, Fujita K, Tabuchi Y, Ikari A, Takeshima H and Sakai H: Crosstalk between Na(+),K(+)-ATPase and a volume-regulated anion channel in membrane microdomains of human cancer cells. Biochim Biophys Acta Mol Basis Dis 1864: 3792-3804, 2018.
54. Zhang HY, Xu WQ, Zheng YY, Omari-Siaw E, Zhu Y, Cao X, Tong SS, Yu JN and Xu XM: Octreotide-periplocymarin conjugate prodrug for improving targetability and anti-tumor efficiency: Synthesis, in vitro and in vivo evaluation. Oncotarget 7: 86326-86338, 2016.
55. Gordy C and He YW: The crosstalk between autophagy and apoptosis: Where does this lead? Protein Cell 3: 17-27, 2012.
56. Liu Y, Shoji-Kawata S, Sumpter RM Jr, Ginet V, Zhang L, Posner B, Tran KA, Green DR, Xavier RJ, Shaw SY, *et al*: Autosis is a Na+,K+-ATPase-regulated form of cell death triggered by autophagy-inducing peptides, starvation, and hypoxia-ischemia. Proc Natl Acad Sci USA 110: 20364-20371, 2013.
57. Liu Y and Levine B: Autosis and autophagic cell death: The dark side of autophagy. Cell Death Differ 22: 367-376, 2015.
58. Zhang K, Chen J, Zhou H, Chen Y, Zhi Y, Zhang B, Chen L, Chu X, Wang R and Zhang C: PU.1/microRNA-142-3p targets ATG5/ATG16L1 to inactivate autophagy and sensitize hepatocellular carcinoma cells to sorafenib. Cell Death Dis 9: 312, 2018.
59. Mukhopadhyay S, Panda PK, Sinha N, Das DN and Bhutia SK: Autophagy and apoptosis: Where do they meet? Apoptosis 19: 555-566, 2014.